(NASA-CR-165316) TECHNOLOGY DEVELOPMENT FOR PHOSPHORIC ACID FUEL CELL POWERPLANT (PHASE 2) Quarterly Report (Energy Research Corp., Danbury, Conn.) 52 p HC A04/MF A01 CSCL 10A

N81-21547

Unclas
G3/44 42079

DOE/NASA/0067-79-2
NASA CR-165316

TECHNOLOGY DEVELOPMENT FOR PHOSPHORIC ACID FUEL CELL POWERPLANT (PHASE II): 5TH QUARTERLY REPORT

LARRY CHRISTNER
ENERGY RESEARCH CORPORATION
3 GREAT PASTURE ROAD
DANBURY, CONNECTICUT 06810

DECEMBER 1979

PREPARED FOR
NATIONAL AERONAUTICS AND SPACE ADMINISTRATION
LEWIS RESEARCH CENTER
CLEVELAND, OHIO 44135
UNDER CONTRACT DEN3-67

FOR
U.S. DEPARTMENT OF ENERGY
ENERGY TECHNOLOGY
DIVISION OF FOSSIL FUEL UTILIZATION
WASHINGTON, D.C. 20545
UNDER INTERAGENCY AGREEMENT DE-AI-03-79 ET11272

NOTICE

Contributors to this Report

Dr. Mohammad Farooque

Mr. Dana Kelley

Mr. Matt Lambrech

Dr. Chang Lee

Dr. Hans Maru

Mr. Sudhakar Perkari

Mr. Michael Puskar

EXECUTIVE SUMMARY

Significant progress made during the quarter for each of the program tasks is summarized below.

Component Development

- A large batch ball milling technique has proved effective for preparing acceptable silicon carbide matrix slurries; these slurries have been cast into matrices which perform as well as previous small batch preparations.
- A technique for fabrication of acid inventory control members has been successfully tested. Further development is in progress.
- Bipolar plates with the more corrosion resistant Varcum resin can be routinely fabricated.

Material Evaluation

- Bipolar plate materials with lower than 50% electrical resistance have been tested. Contact resistance has also been identified as a potentially large contributor to the observed stack resistance.
- Electrochemical corrosion parameters for low resin content materials (having low electrical resistance) have been determined.

Endurance Testing

- Twelve stacks built to examine long-term endurance (10,000 hours) have completed approximately 2000 hours of testing. The SiC and MAT-1 matrix cells appear to be more stable than the Kynol matrix stacks. Performance, although 10 to 20 mV lower than the peak performance, appears to be stable for SiC and MAT-1 stacks.

- A 350 cm^2 stack (No. 379), with over 6000 hours of operation and an average cell voltage of 0.61V at 100 mA/cm^2, appears to be very stable.

Short Stack Testing

- A 1200 cm^2 (12 in. x 17 in.) 5 cell stack (No. 407) was operated for over 1000 hours. This stack, however, required frequent acid additions. Improvements are being made in the cell design and assembly procedures to rectify this problem.

Long Stack Testing

- An improved 23 cell, 1200 cm^2 stack has been built and tested. Improvements include X-type compression bar assembly, fuel inlet diffuser, and a startup procedure designed to reduce acid volume changes. An average cell voltage of 0.56V at 100 mA/cm^2 and 177°C has been achieved.
- A reformer test facility capable of producing sufficient hydrogen for a 2kW stack has been built. It has been checked out with both propane and methane.

TABLE OF CONTENTS

Section		Page No.
	EXECUTIVE SUMMARY	i
TASK I	COMPONENT DEVELOPMENT	1
1.1	MATRIX DEVELOPMENT	1
1.2	COMPONENT SCALE-UP	1
1.3	DEFINITION AND CONTROL OF ELECTROLYTE VOLUME CHANGES	4
1.4	BACKING PAPER TECHNOLOGY	5
1.5	BIPOLAR PLATE TECHNOLOGY	7
1.5.1	Molding	7
1.5.2	Carbonization	7
TASK II.	MATERIAL EVALUATION	8
2.1	COMPONENT CORROSION RESISTANCE	8
2.1.1	Chemical Corrosion Measurement	8
2.1.2	Electrochemical Corrosion Measurement	9
2.2	PHYSICAL PROPERTY MEASUREMENTS	15
2.2.1	Electrical Resistivity of Composite Materials	15
2.2.2	Electrical Resistance of Bipolar Plates	17
TASK III.	ENDURANCE TESTING	19
3.1	MEASUREMENT OF P_4O_{10} VAPOR CONCENTRATION	19
3.2	EFFECT OF OPERATING VARIABLES ON CELL PERFORMANCE AND COMPONENT DEVELOPMENT	19
3.3	TEN-THOUSAND HOUR ENDURANCE STACKS	21

TABLE OF CONTENTS (concluded)

Section		Page No.
TASK IV.	SHORT STACK TESTING	24
4.1	CURRENT COLLECTING POSITIONS IN THE STACK	24
TASK V.	LONG STACK TESTING	28
5.1	A 2kW STACK	28
5.2	THERMAL STACK EXPANSION/CONTRACTION	37
5.3	REFORMER TESTING	39

LIST OF FIGURES

Section		Page No.
TASK II.	MATERIAL EVALUATION	
II.1	True Corrosion and Acid Absorption Characteristics of Pure Resins	10
II.2	Polarization Plot of the Varcum Composite	11
II.3	Change in the Theoretical Open Circuit Carbon Corrosion Potential with Temperature for Various Acid Concentrations	14
II.4	Four Point Resistivity Measurements of Colloid 8440/Asbury A-99 Graphite Composites	16
TASK IV.	SHORT STACK TESTING	
IV.1	Bipolar Plate Design Modification	26
IV.2	Stack Current Collecting Positions	28
TASK V.	LONG STACK TESTING	
V.1	Second 2kW Stack Assembly	29
V.2	Fuel Diffuser in Fuel Manifold	30
V.3	Acid Wicking in 23-Cell Stack and a Phenolic Matrix Strip	32
V.4	History of Stack 410 Operation	35
V.5	Performance Characteristics with Running Time for 2nd 2kW Stack	36
V.6	Temperature Profiles on Center Planes of 2kW Stack (measured at E=12.90V and I=112A)	38
V.7	Thermal Characteristics in Propane Reforming at a Flow Rate of 1.0 lpm	40
V.8	Thermal Characteristics in Propane Reforming at a Flow Rate of 1.5 lpm	41

LIST OF TABLES

Section		Page No.
TASK I.	COMPONENT DEVELOPMENT	
I.1	The 25 cm^2 Cell Testing Summary	2
TASK II.	MATERIAL EVALUATION	
II.I	Kinetic Parameters of the Electrochemical Corrosion Reaction	12
II.2	Electrical Resistance of 1200 cm^2 Bipolar Plates	18
TASK III.	ENDURANCE TESTING	
III.1	Summary of Acid Loss Experiments	20
III.2	Summary of Performance for 10,000 Hr Endurance Stacks	22
TASK IV.	SHORT STACK TESTING	
IV.1	Summary of 5 Cell, 1200 cm^2 Stack Testing	25
TASK V.	LONG STACK TESTING	
V.1	Test Summary of 2kW Stack (No. 410)	33-34
V.2	Thermal Expansion for a 23-Cell Stack	37
V.3	Comparison of Experimental Compositions with Equilibrium Calculation for Propane Performing	42
V.4	Comparison of Reformed Product Compositions Obtained by Experiment and by Equilibrium Calculation for Methane Reforming	43

TASK I. COMPONENT DEVELOPMENT

1.1 MATRIX DEVELOPMENT

Efforts to produce mechanically stronger and more porous SiC matrices continue. The 25 cm^2 test cells containing matrices made with a 2.5% Polyox inking vehicle (vs the standard 1/2% solution) were terminated (Table I.1, Cells 1381 and 1386) after sufficient time to demonstrate that there was no poisoning effect due to a possible increase in residual Polyox. These and previous cells with identical matrices have shown average or above average performance with matrix porosities in excess of 60%. The 2.5% Polyox SiC matrix will next be tested in a 300 cm^2 stack.

Another cell was built (Table I.1, Cell 1409) to evaluate the effect, if any, of ball milling the SiC slurry used to cast the matrix. Previously SiC slurries were made up individually for each matrix through a combination of hand mixing and mixing on a magnetic stirrer. Ball milling has been used to make the slurry in the quantity and rates necessary for rapid production of large (1200 cm^2) matrices. Ball milling produces a smooth, uniform slurry without excessive degradation of the shear sensitive inking vehicle. So far Cell 1409's performance (660 mV at 200 mA/cm^2 IR Free) has been excellent. This modification in the procedure therefore appears acceptable.

1.2 COMPONENT SCALE-UP

Production of 1200 cm^2 components has greatly increased during this quarter. The new larger rolling mill has been producing seamless rolled electrodes and more than 80 large sheet mold electrodes have also been produced during this period. In addition, more than two dozen rolled and sheet mold electrodes (1200 cm^2) have been coated with SiC matrices. Stack 412 contains both electrode types and SiC matrices. During the stack startup period, every cell is producing a minimum of 600 mV

ENERGY RESEARCH CORPORATION

ENERGY RESEARCH CORPORATION

TABLE I.1

THE 25 cm^2 CELL TESTING SUMMARY (Page 1 of 2)

CELL NO.	1381	1386	1409	1426
TEST OBJECTIVE	2.5% Polyox in Matrix	2.5% Polyox in Matrix	Ball Milled SiC Matrix	Prewashed Backings
CELL CHARACTERISTICS				
ANODE				
Type	Rolled	Rolled	Rolled	Sheet Mold
TFE, %	40	40	40	40
Loading, mg Pt/cm^2	0.3	0.38	0.49	0.29
CATHODE				
Type	Rolled	Rolled	Rolled	Sheet Mold
TFE, %	40	40	40	40
Loading, mg Pt/cm^2	0.5	0.54	0.53	0.7
MATRIX	SiC	SiC	SiC	Kynol
TFE, %	4	4	4	-
Porosity, %	63	-	-	-
Thickness, cm	0.015	0.015	0.013	0.048
Sintering	15 min @ 330°C	15 min @ 330°C	15 min @ 330°C	-
ANODE BACKING % FEP	38	36	38	32.7
CATHODE BACKING % FEP	38	40	38	30.5
PEAK PERFORMANCE, mV IR-Free				
AIR - 100 mA/cm^2	670	718	710	650
200 mA/cm^2	620	675	660	590
O_2 - 100 mA/cm^2	745	788	780	710
200 mA/cm^2	695	755	730	670
O_2 GAIN - 100 mA/cm^2	75	70	70	60
200 mA/cm^2	75	80	70	80
PRESENT PERFORMANCE AIR - 200 mA/cm^2	*	*	640	590
CELL LIFE, hours	1512	2016	984	240

* Test Terminated

ENERGY RESEARCH CORPORATION

ENERGY RESEARCH CORPORATION

TABLE I.1

The 25 cm^2 CELL TESTING SUMMARY (Page 2 of 2)

CELL NO.	1345	1374	1378	1384
TEST OBJECTIVE	Large Sheet Mold Electrodes	AICM	AICM	Pre-filled Low FEP Backing
CELL CHARACTERISTICS				
ANODE				
Type	Sheet Mold	Rolled	Rolled	Rolled
TFE, %	40	40	40	40
Loading, mg Pt/cm^2	0.45	0.3	0.3	0.3
CATHODE				
Type	Sheet Mold	Rolled	Rolled	Rolled
TFE, %	40	40	40	40
Loading, mg Pt/cm^2	0.5	0.5	0.5	0.5
MATRIX	Kynol	SiC	SiC	SiC
TFE, %	-	4	4	4
Porosity, %	-	-	-	-
Thickness, cm	0.048	0.015	0.015	0.015
Sintering	-	15 min @ 330°C	15 min @ 330°C	15 min @ 330°C
ANODE BACKING % FEP	35	13	11.6	20
CATHODE BACKING % FEP	34	34	39	39
PEAK PERFORMANCE, mV IR-Free				
Air - 100 mA/cm^2	705	665	705	675
200 mA/cm^2	666	600	650	620
O_2 - 100 mA/cm^2	765	725	770	735
200 mA/cm^2	735	645	740	695
O_2 GAIN - 100 mA/cm^2	60	60	65	60
200 mA/cm^2	75	45	90	75
PRESENT PERFORMANCE				
AIR - 200 mA/cm^2	670	*	540	*
CELL LIFE, hours	4272	2376	2640	1740

* Test Terminated

(terminal voltage) at 100 mA/cm^2. Large sheet mold electrodes were previously tested in Stack 409.

1.3 DEFINITION AND CONTROL OF ELECTROLYTE VOLUME CHANGES

A long-term experiment has been conducted to measure the effect of an AICM on cell performance using:

Cell 1374 with a selectively wetproofed anode backing. (Refer to Table I.1 for all cells.)

Cell 1384 with a prefilled anode containing 20% FEP in its backing.

Cell 1345 with sheet mold electrodes and a phenolic fiber matrix (being used as a control).

After an initial conditioning period, the cells were placed on a reduced acid addition schedule. The control cell (No. 1345) has shown classic responses to acid depletion followed by acid addition. As the cell dries out, its OCV and performance at load begin to drop and the cell's internal resistance (IR) increases. When acid is added, the cell's OCV and performance at load increase and the cell's IR drops. The changes in cell IR correlate closely with changes in its performance. Cell 1345 is still running and is now being deprived of acid for an extended period of time to determine how long it can continue and also the extent of recovery from acid addition after it has dropped to a very low performance level. Cell 1374, which contains only 13% FEP in its anode backing, exhibited extremely stable performance during most of the test period, even when the time interval between acid additions was twice that of the control cell. This is precisely the kind of performance desired in an AICM cell. Cell 1374 was damaged by equipment failure and has been terminated. Cell 1384, which contains 20% FEP uniformly distributed throughout its anode backing, falls somewhere between the control and Cell 1374 in terms of response to acid addition. Its performance was

not as stable as that of Cell 1374 and its responses to acid additions were not as marked as those of Cell 1345. Cell 1384 failed due to a short. Tests of this type will be repeated and expanded to include simulated load cycling, temperature variation and humidification of gases.

Another test of a selectively wetproofed anode backing as an AICM was performed on Cell 1378 (Table I.1). Despite containing only 11.6% FEP in its anode backing, the O_2 gains are acceptable and the performance has been excellent (650 mV at 200 mA/cm^2, IR free), but is now deteriorating due to a short. Attempts to eliminate the short have not been successful. However the cell has been kept running because after 2640 hours, backing flooding has still not become a problem, despite the low FEP content. This demonstrates that selectively wetproofed backings can work as AICMs if the wetproofing pattern is well chosen and carefully applied.

1.4 BACKING PAPER TECHNOLOGY

During the FEP treatment of backings, a significant amount of black, particulate material has been observed to wash out of the carbon paper. It may be assumed that some of this material is retained in the backings after treatment. The presence of this material is disturbing even if it is only carbon, because loose carbon particles may increase the wettability of the backing paper. Moreover, scanning electron microscope (SEM) pictures and X-ray microanalysis have indicated that many particles in untreated backings contain inorganic compounds of zinc and other metals which could act as catalyst poisons if allowed to remain in the backings. A number of backings intended for sheet mold electrodes were prewashed in a dilute FEP emulsion to remove the particulate material. After a great deal of the black material was removed in this manner, the backings were then treated with FEP in the usual way and sintered.

Acid pick-up tests to determine the wettability of a prewashed backing vs a standard backing provided some surprises. Small pieces of 1200 cm^2 backings were float filled in 102% H_3PO_4 at 177°C. The prewashed backing contained 31.3% FEP and the standard backing contained 34.4% FEP. The amount of acid picked up indicates that wetting differences were greater from place to place on each backing (up to 1400%) than between identical locations on the two backings (about 26%). Furthermore the acid pick-up in the wettest areas was high enough to cause some concern about flooding in an actual cell test. The most plausible explanation for this behavior at present is that the procedure used in the FEP treatment produces localized variations in FEP content.

An attempt was made to verify this theory by placing drops of acid in various places across the same two backings used in the previous tests. The backings were placed in a 177°C oven and the contact angle was observed between the drops of acid and the backings. The lower FEP content, prewashed backing showed visibly smaller contact angles (indicative of greater wettability) than the standard backing. However no significant differences were detected in the contact angles among the drops on each backing. This is contrary to what might have been expected from the acid pick-up tests. Additional work is planned to resolve this question.

A 25 cm^2 test cell (Table I.1, Cell 1426) was built with pieces of 1200 cm^2 sheet mold electrodes on prewashed backings. The FEP content of the backings is lower than normal (32.7 and 30.5% FEP) and the performance (590 mV at 200 mA/cm^2, IR Free) is also lower than normal. However the O_2 gains are low and indicate that the cell is not flooded. Additional testing is required to determine why cell performance is so low, but it does not appear to be related to the backings.

1.5 BIPOLAR PLATE TECHNOLOGY

1.5.1 Molding

Fabrication of 1200 cm^2 bipolar plates with 32 wt% Varcum 24-655 resin/68 wt% Asbury A-99 graphite was successful. Production rates were comparable to the current bipolar plates with 33 wt% Colloid 8440 resin and 67 wt% graphite.

A 3 cell stack (No. 614) with 350 cm^2 bipolar plates (32 wt% Varcum 24-655/68 wt% A-99) is currently being assembled. The cell resistance and conditions of these new plates will be monitored.

1.5.2 Carbonization

A retort was designed for carbonizing 1200 and 350 cm^2 bipolar plates. A successful carbonization heating cycle, previously reported for 175 cm^2 sections of bipolar plates, will be evaluated for the 1200 and 350 cm^2 plates.

The retort and furnace used for developing the heating cycle for the 175 cm^2 sections is now being utilized in developing a heating cycle for the thicker plates for 25 cm^2 cells. To eliminate blistering of the thicker plates, a slower heating cycle is needed (e.g., 1°C/hr between 250 and 350°C for plates 0.5 cm thick).

TASK II. MATERIAL EVALUATION

2.1 COMPONENT CORROSION RESISTANCE

2.1.1 Chemical Corrosion Measurement

A. Evaluation of Mixed Composites:

To improve the corrosion resistance of Colloid (a thermoset resin), a compatable Resin No. P-1 was added and the bipolar plates were fabricated by hot compression molding of this graphite/Colloid/Resin P-1. A recommended temperature cycle was used to sinter the graphite/Colloid/Resin P-1. Samples with three different amounts of resin were thus prepared and tested in subsequent corrosion experiments. The results indicate that increasing the resin content of the sample leads to more acid absorption. This is probably due to an increase in cracks, voids, and surface defects of the samples caused by insufficient wetting and/or poor flow characteristics. Conversely, these results point out that by adding a small amount of resin in this experiment the acid absorption and corrosion characteristics of the Colloid based composites can be changed significantly. There is probably an "optimum" proportion of resin which should be added during the Colloid composite fabrication process. Resin P-1 is expected to fill in the defects, cracks and pores which are otherwise present in Colloid based samples. In this study, no attempt has been made to find this optimum resin value. In future experiments, resin P-1 will be alloyed with Varcum based composites to find its potential for suppressing the corrosion rate of the latter.

B. Corrosion Characteristics of Pure Resins:

Only the apparent corrosion rates (prior to correcting for acid absorption) of several pure resins were reported previously*. The initial 2000 hours of controlled experiments with pure resins

*DEN3-67, No. 12, July - Sept. 1979.

were recently completed and the results (evaluated in Figure II.1) reveal that:

- The true corrosion rates of Colloid 8440, Varcum 24-655 and Plenco 402 differ only slightly. Their approximate true corrosion rate is -1.25 μg/hr-cm^2.
- Plenco 402 and Colloid 8440 samples absorbed significant amounts of acid. Because of the scatter in the acid absorption data collected so far, the true acid absorption rates of the samples are difficult to define at this stage.
- Varcum 24-655 samples did not absorb acid.

2.1.2 Electrochemical Corrosion Measurement

Electrochemical corrosion behavior of 22% Plenco 402 and 22% Varcum 29703 based composites was evaluated at four different temperatures and at potentials between 0.55 and 1.0V. Representative corrosion polarization plots of the Varcum sample, taken at temperatures of 190 and 167°C, are shown in Figure II.2*. It is apparent from this plot that the expected overall half cell carbon corrosion reaction represented as:

$$C\ (S) + 2H_2O\ (\ell) \rightarrow CO_2\ (g) + 4H^+ + 4e^-\ ;\ E_{0,\ 25°C} = 0.21V$$

shows two different reaction mechanisms in the potential range of this study. It is also apparent from the Tafel plots of the figure that a third reaction pathway may be present between the rest potential and 0.6V (RHE); this will be investigated in future experiments. Reported in Table II.1 are: Tafel slopes, b; transfer coefficients, $\overleftarrow{\alpha}$; exchange current densities, i_o; and energy of activation, ΔE of the electrochemical reaction of the two samples, representative of each of the mechanisms. The ΔE

*Ascending and descending V - log i plots are observed to be slightly different, suggesting a hysteresis between them. Results of Figure II.2 and Table II.2 correspond to the descending portion of the V - log i plot.

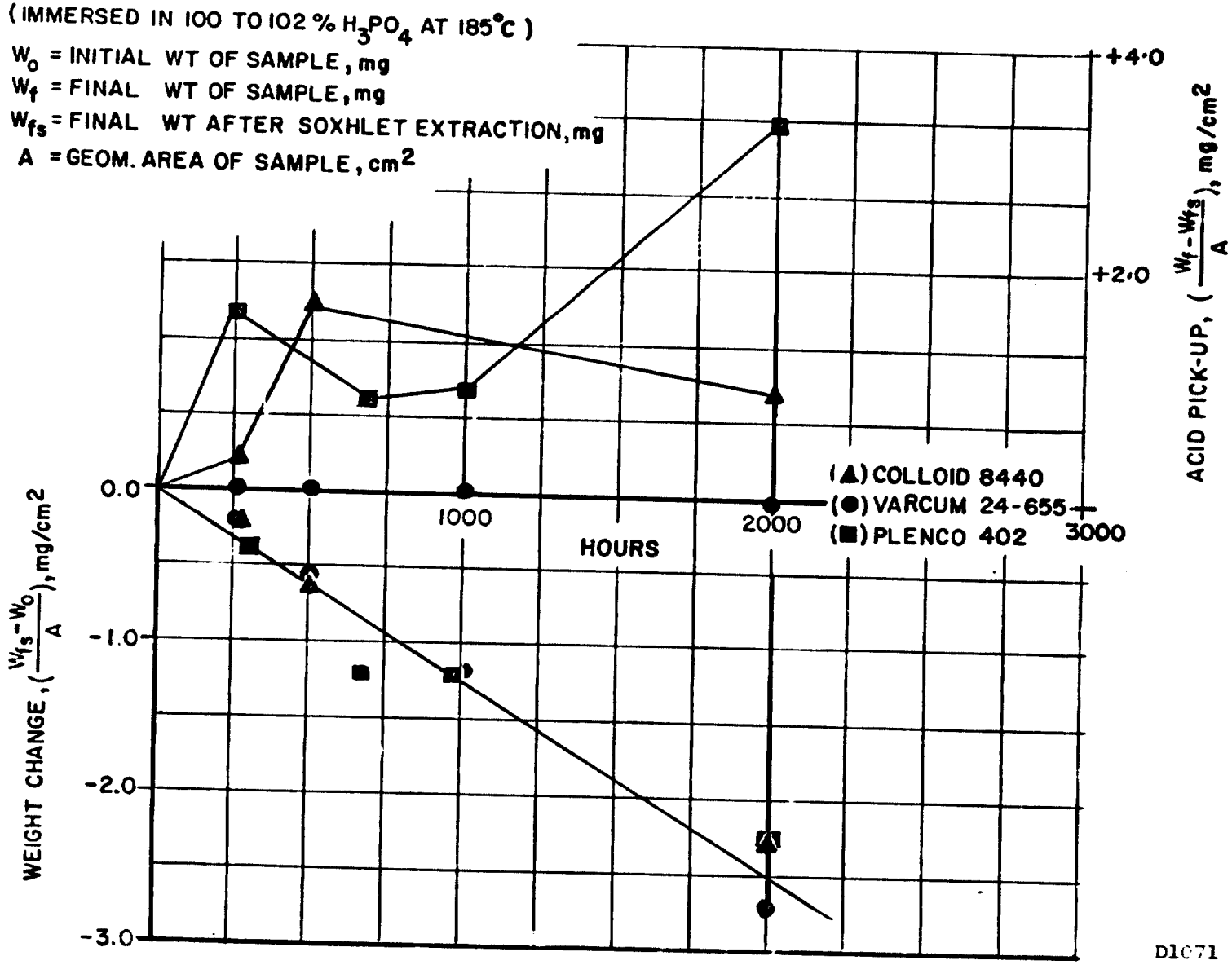

FIGURE II.1 TRUE CORPOSION AND ACID ABSORPTION CHARACTERISTICS OF PURE RESINS

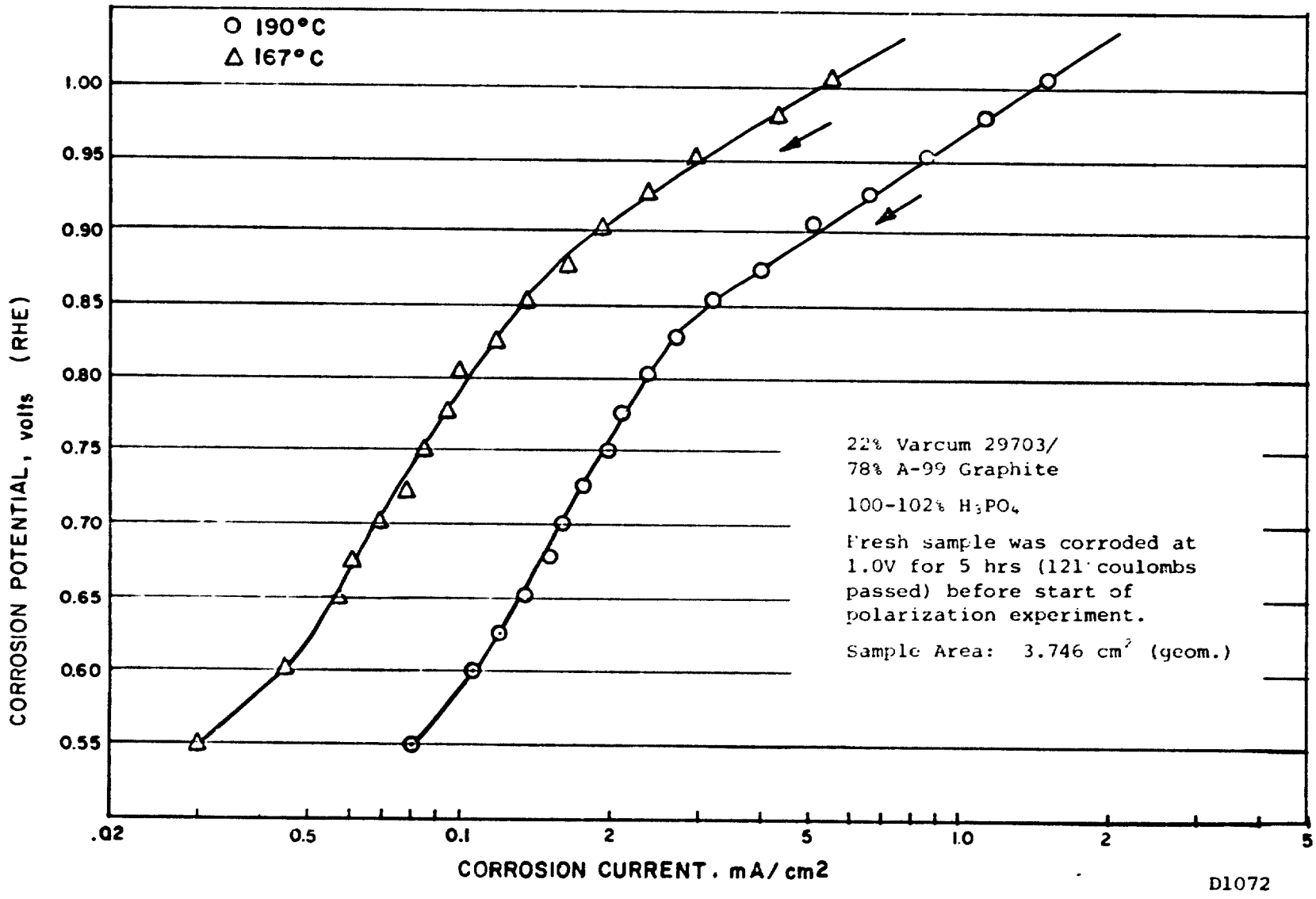

FIGURE II.2 POLARIZATION PLOT OF THE VARCUM COMPOSITE

TABLE II.1 KINETIC PARAMETERS OF THE ELECTROCHEMICAL CORROSION REACTION

SAMPLE	TEMPERATURE, °C	BETWEEN 0.60 and 0.80V (RHE)				BETWEEN 0.825 and 1.0V (RHE)			
		TAFEL SLOPE $b = \frac{RT}{\alpha F} \times 2.303$ V/decade	TRANSFER COEFFICIENT α	EXCHANGE CURRENT DENSITY i_o (A/cm^2) x 10^6	ACTIVATION ENERGY, ΔE kcal/mol K	TAFEL SLOPE $b = \frac{RT}{\alpha F} \times 2.303$ V/decade	TRANSFER COEFFICIENT α	EXCHANGE CURRENT DENSITY i_o (A/cm^2) x 10^6	ACTIVATION ENERGY, ΔE kcal/mol K
22% Plenco 402 + 78% A-99 Graphite	190.0	0.625	0.147	37.6	10.1	0.299	0.310	1.98	11.25
	183.4	0.590	0.154	32.9		0.309	0.290	2.30	
	167.8	0.531	0.160	23.0		0.297	0.290	1.20	
22% Varcum 29703 + 78% A-99 Graphite	190.0	0.586	0.156	16.2	13.1	0.222	0.417	0.16	10.90
	183.3	0.600	0.152	15.2		0.231	0.400	-	
	173.9	0.575	0.154	10.9		0.280	0.320	0.18	
	166.7	0.540	0.161	6.6		0.231	0.378	0.11	

is calculated from the slope of the ln i_o vs $\frac{1}{T}$ plot. E_T, the theoretical open circuit corrosion potential (TOCP) used for evaluation of the exchange current densities was calculated using:

$$E_T = E_o + \frac{RT}{4F} \ln \frac{a^2_{H_2O\ (\ell)}}{a_{CO_2\ (g)} \times a^2_{H_2\ (g)}}$$

assuming that the electrolyte present on the surface of the sample is saturated with CO_2. Figure II.3 illustrates the TOCP for the carbon corrosion reaction corresponding to the fuel cell operating conditions. As expected, because of higher water activity, the corrosion potential is more anodic in the dilute acids.

The following important observations can be made from the calculated electrochemical parameters, as reported in Table II.2.

- Tafel slopes and transfer coefficients differ in two different potential regions.
- As expected, Tafel slopes increase with temperature. Activation energies for both reactions are between 10 and 13 kcal/mol K.

The kinetic parameters, especially α and ΔE, would enable us to predict the corrosion rates corresponding to other operating temperatures and potentials for which the experimental results are not available. As an example, according to the calculations shown below, at a cathode potential of 0.75V, the expected 22% Varcum bipolar plate corrosion rate, i_2, at 190°C in 100% acid is expected to be about twice the corrosion rate, i_1, observed at 177°C and at 0.65V cathode potential.

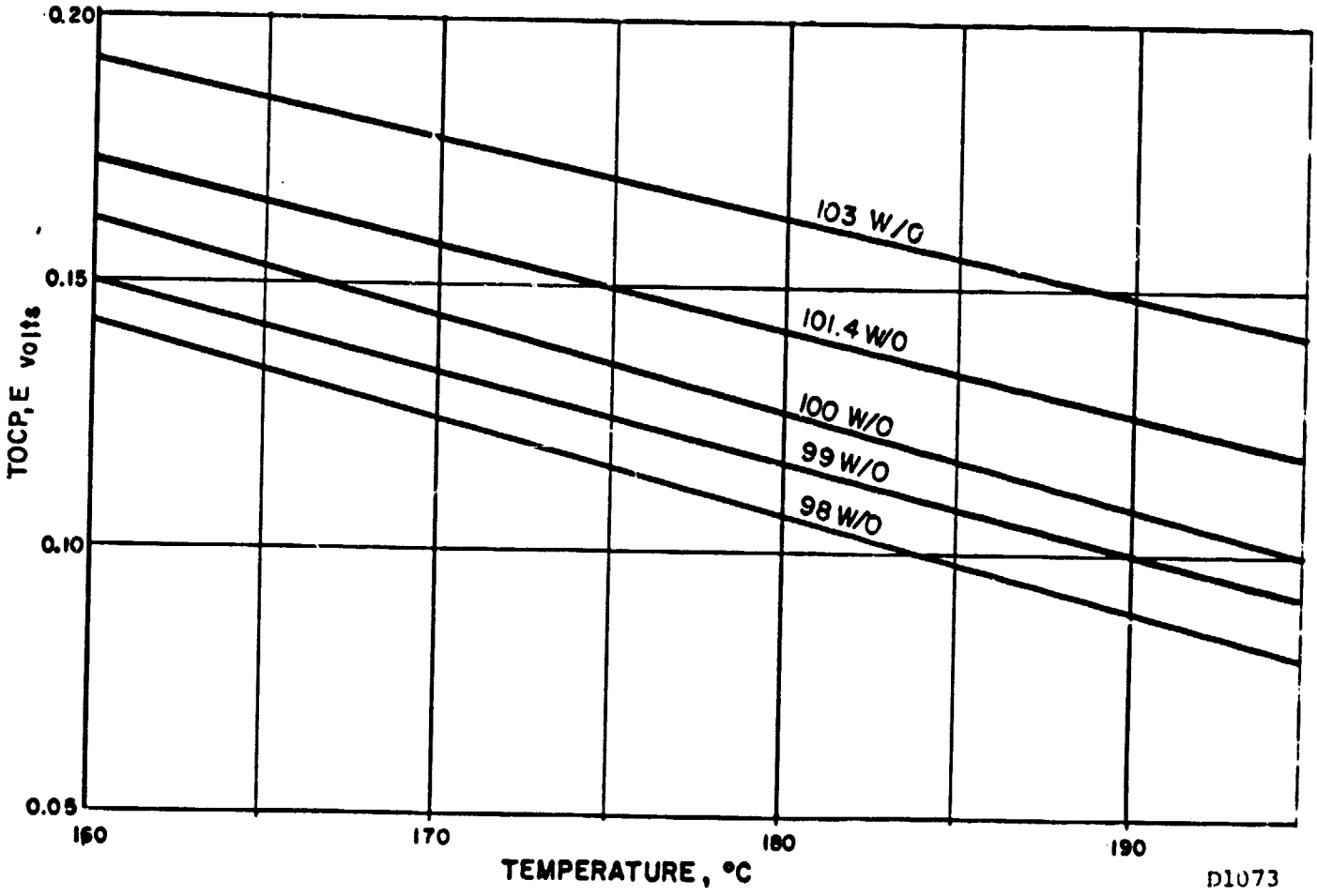

FIGURE II 3 CHANGE IN THE THEORETICAL OPEN CIRCUIT CARBON CORROSION POTENTIAL WITH TEMPERATURE FOR VARIOUS ACID CONCENTRATIONS

$$\frac{i_2}{i_1} = e^{-\frac{\Delta E}{R}\left(\frac{1}{T_2} - \frac{1}{T_1}\right)} \times e^{\frac{\alpha F}{R}\left[\frac{V_2 - E_{T_2}}{T_2} - \frac{V_1 - E_{T_1}}{T_1}\right]}$$

$$= e^{-\frac{13.1 \times 10^3}{1.987}\left(\frac{1}{463} - \frac{1}{450}\right)} \times e^{\frac{0.154 \times 96493}{8.31}\left[\frac{0.75 - 0.11}{463} - \frac{0.65 - 0.13}{450}\right]}$$

$$= 2.05$$

2.2 PHYSICAL PROPERTY MEASUREMENTS

2.2.1 Electrical Resistivity of Composite Materials

The electrical resistivity of phenolic resin/graphite plate materials with Varcum 24-655 and Colloid 8440 resins was measured by a four point method. The results confirm the anisotropic nature of the materials (Figure II.4). The phenolic resin/graphite composites were compression molded. Cylindrical samples were machined from the molded parts for two orientations: an axis parallel to the pressing direction and an axis perpendicular to the pressing direction. Electrical contacts were connected to the ends of the cylinders and the electrical resistivity measured. The parallel to pressing samples had electrical resistivity 3 to 4 times greater than samples perpendicular to pressing. The current in a fuel cell stack flows parallel to pressing. From the results in the parallel to pressing direction, the values of electrical resistivity for Varcum 24-655 material appear to be 10 to 20% lower than the Colloid 8440 materials. Electrical resistivity values for Varcum 24-655 or Colloid 8440 materials with Asbury A-99 graphite were approximately 10 to 30% lower than with a mixture of 27 wt% Asbury 850 and 73 wt% Asbury A-99 graphite. Asbury A-99 graphite is an artificial graphite with 5 to 44 μm particles and Asbury 850 graphite is a natural graphite with 0.5 to 0.6 μm particles.

Future electrical measurements shall emphasize development of methods to determine the electrical contact resistance between

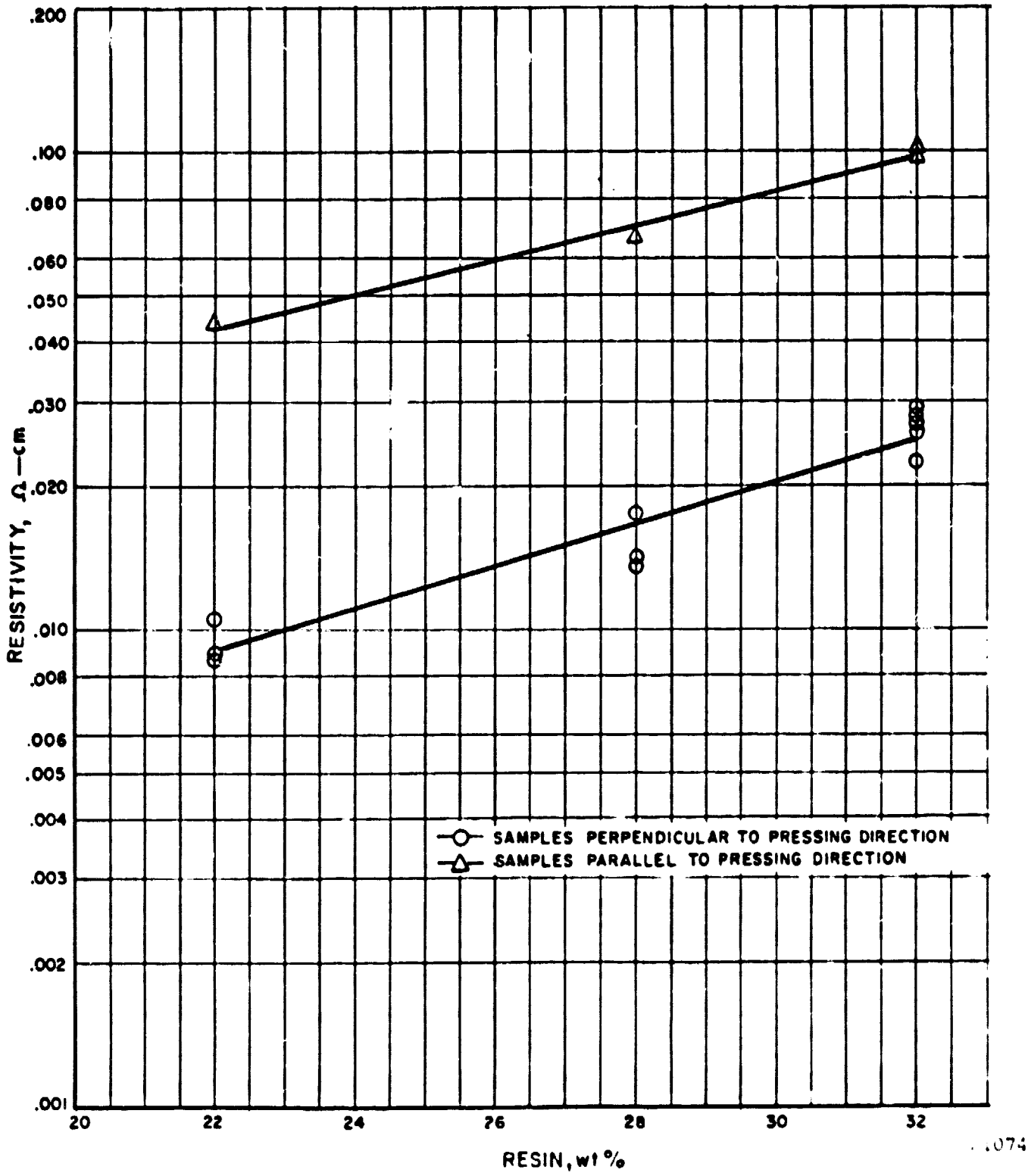

FIGURE II.4 FOUR POINT RESISTIVITY MEASUREMENTS OF COLLOID 5440/ ASBURY A-99 GRAPHITE COMPOSITES

fuel cell components using a four point method.

2.2.2 Electrical Resistance of Bipolar Plates

The contributions of the electrical resistance and millivolt drop as a function of the electrical resistivity of the bipolar plate were estimated this quarter. Table II.2 shows the estimated resistance contributions of the bipolar plates and DIGAS coolers in a 23 cell, 1200 cm^2 cell stack. The resistivity values represent an estimated range of values for phenolic resin/graphite materials. For 33 wt% Colloid 8440/67 wt% A-99 and 850 graphite the current estimate for electrical resistivity is 0.15 ohm-cm. Comparing the calculated value of resistance at 0.15 ohm-cm resistivity to stack measurements, the bipolar plates account for about 20% of stack resistance. The identification and techniques to measure the "other" resistances will begin with the development of methods to measure contact resistance.

TABLE II.2 ELECTRICAL RESISTANCE OF 1200 cm^2 BIPOLAR PLATES

ESTIMATED MEASUREMENTS OF	RESISTANCE, mΩ			PERFORMANCE DROP @ 113AMP, mV		
	RESISTIVITY, Ω -cm			RESISTIVITY, Ω -cm		
	0.05	0.15	0.30	0.05	0.15	0.30
Bipolar Plate	0.03	0.09	0.19	3.55	10.63	21.26
DIGAS Cooler	0.06	0.20	0.40	7.48	22.44	44.88
23 Cell Stack, 4 DIGAS Coolers and 20 Bipolar Plates	0.89	2.68	5.35	100.7	302.3	604.7
Actual Measurements on 23 Cell Stack (No. 410)	12.5			1413		

TASK III. ENDURANCE TESTING

3.1 MEASUREMENT OF P_4O_{10} VAPOR CONCENTRATION

Acid loss experiments conducted during this quarter are summarized in Table III.1. At the 7th experiment, it was confirmed that graphite/resin plates used in the experiment were losing significant weight with time at 195°C. This explains the higher P_4O_{10} concentration shown by cell component weight at the 5th experiment. Higher P_4O_{10} concentration in the collected acid vapor was also found, due to channel flooding by the acid, from which some amount of acid was pushed into vapor collecting tubes. The optimum amount of acid filling in the 25 cm^2 cell was found to be approximately 1.5 g of 101% acid at 30°C humidification to minimize channel flooding. At the 6th experiment, inlet air was not humidified, resulting in highly concentrated acid (~110%) in the cell. At this concentration, higher P_4O_{10} vapor pressure was anticipated. As expected, 0.4 ppm of P_4O_{10} vapor was obtained and 0.3 ppm from the 104% acid cell (7th experiment) at an air flow of 500 cc/min and a cell temperature of 195°C. In the previous quarterly, 0.26 ppm was reported at 500 cc/min air flow and 180°C (97.5 % acid in the cell). These experiments provide concentration effect on acid loss. In the next quarter, flow effect will be further investigated to determine saturated flow condition. For the next experiment, graphite/resin plates are being further heat-treated at 200°C until no more weight loss is encountered. All the new plates have been coated with polyether sulfone (PES) to prevent acid absorption. More reliable results are expected for the next quarter and the projected acid loss will be compared with actual loss in a 350 cm^2 stack.

3.2 EFFECT OF OPERATING VARIABLES ON CELL PERFORMANCE AND COMPONENT DEVELOPMENT

The three stacks reported here were assembled with sheet molded electrodes and rolled electrodes. Stack 379 was assembled

TABLE III.1 SUMMARY OF ACID LOSS EXPERIMENTS

RUN NO.	CELL CONDITIONS			P_4O_{10} CONCENTRATION, ppm		COMMENTS
	AIR FLOW, cc/min	HUMIDIFICATION, °C	CELL TEMP. °C	By COMPONENT WT.	By CONDENSED VAPOR	
5	400	50	190	1.75	1.2	Humidified cathode side only. Acid Conc. = 106% Hours run = 240
6	500	-	195	*	0.4	Acid Conc. = 110% Hours run = 432
7	500	30	195	*	0.3	Humidified both sides. Acid Conc. = 104% Hours run = 360

* Significant weight loss in plates.

with sheet mold electrodes and Kynol matrix whereas Stack 380 was assembled with rolled electrodes and a SiC matrix. The performance of Stack 379 at the end of the quarter (6245 hours) is 0.61V/cell at 100 mA/cm^2. The performance of Stack 380 is 0.5V/cell at 5667 hours of operation. These stacks were assembled with prefilled components and started operating the following day. For a stack assembled with dry components, about 10 days of wicking time is required before operating the stack. The same wet assembly procedure will be followed in assembling a few full scale stacks to establish wet assembly procedures. Stack 379 also establishes the long-term operating capability of sheet mold electrodes. Another stack which has 2814 hours of operating time with sheet mold electrodes and SiC matrix is Stack 391.

3.3 TEN-THOUSAND HOUR ENDURANCE STACKS

A major emphasis was placed on stack startup and operation during this quarter. The components in these 350 cm^2 stacks are as approved by the NASA/Lewis Program Manager. These stacks are basically divided into three types, depending on the matrices (Kynol, SiC and MAT-1, as noted in Table III.2). As shown in the table, two different platinum loadings, 0.8 and 0.6 mg/cm^2, have been used in these stacks. Stack performance at 100 mA/cm^2 is reported on the 15th of each month during the quarter. While most of the endurance stacks exhibited fairly stable performance, the stacks with Kynol matrices appeared to decrease slightly in performance. Stacks 396, 604, 610 and 611 decreased from 10 to 30 mV in performance. The reason for this decrease is being analyzed carefully for appropriate action. The loss in stack performance can be attributed to changes in ohmic resistance of the stack and activation and diffusion characteristics of the electrodes. In the process of analyzing these facts, ohmic resistance and polarization curves have been obtained at regular intervals for these stacks. Analysis of ohmic resistance in Stack 396 indicated a decrease of only 12 mV/cell in performance due to increased resistance while a total loss of 30 mV is observed over the entire

ENERGY RESEARCH CORPORATION

TABLE III.2 SUMMARY OF PERFORMANCE
FOR 10,000 HR ENDURANCE STACKS

	TOTAL Pt LOADING mg/cm²	STACK NO.	Oct. 15, 1979		Nov. 15, 1979		Dec. 15, 1979	
			NO. OF HOURS	AVG.* PERF, V (OCV, V)	NO. OF HOURS	AVG.* PERF, V (OCV, V)	NO. OF HOURS	AVG.* PERF, V (OCV, V)
KYNOL	0.6	604	381	0.58 (0.83)	1127	0.56 (0.82)	1862	0.57 (0.83)
		610	52	0.57 (0.83)	614	0.58 (0.82)	1334	0.55 (0.80)
	0.8	396	907	0.60 (0.85)	1651	0.57 (0.82	2347	0.57 (0.82)
		611	23	0.59 (0.86)	575	0.59 (0.86)	1293	0.56 (0.84)
SiC	0.6	605	293	0.60 (0.76)	1032	0.61 (0.77)	1752	0.60 (0.80)
		607	286	0.61 (0.77)	1054	0.61 (0.79)	1680	0.59 (0.78)
	0.8	600	714	0.61 (0.78)	1460	0.60 (0.77)	2176	0.59 (0.80)
		601	603	0.61 (0.77)	1337	0.59 (0.77)	2057	0.60 (0.79)
MAT-1	0.6	608	274	0.60 (0.81)	1008	0.59 (0.80)	1936	0.58 (0.79)
		609	275	0.59 (0.81)	1009	0.58 (0.80)	1739	0.58 (0.79)
	0.8	602	766	0.60 (0.79)	1510	0.59 (0.78)	2302	0.59 (0.79)
		603	694	0.62 (0.79)	1408	0.61 (0.78)	2158	0.61 (0.77)

*@ 100 mA/cm²

period. Analysis of polarization curves at different operating hours resulted in high Tafel slopes. At 100 mA/cm^2, the "O_2 gain" (the potential difference of the cell with oxygen to that of air at 178°C)was about 80 mV. The theoretical O_2 gain for this condition is about 68 mV without any diffusion polarization. The fact that the "O_2 gain" is increasing with the current density, is indicative of diffusion limitation on cathode. The same observations were made with Stack 611 which lost about 30 mV/cell over the period. In most stacks it is observed that the open circuit voltages (OCVs) decrease and ohmic resistances increase, an indication of the need for acid.

Stackswith SiC and Mat-1 matrices are also being analyzed in a similar way; results will be reported in the following reports as appropriate.

TASK IV. SHORT STACK TESTING

Test results of all 1200 cm^2 short stacks operated during this quarter are detailed in Table IV.1. Stack 407 which was disassembled after 1243 hours of operation required consistent addition of acid. Stacks 409, 411 and 412 also showed early crossleaks. All of these stacks were assembled with plates without acid channels. (See Figure IV.1a.) A small strip of anode was cut to facilitate wicking of acid to the matrix. The crossleaks are probably caused by the exposed area of the matrix which has very low bubble pressure especially when slightly dry. To eliminate this problem, the plate design is being modified by incorporating an acid channel. (See Figure IV.1b.)

4.1 CURRENT COLLECTING POSITIONS IN THE STACK

An experiment was conducted on a 5 cell, 1200 cm^2 stack to test the minimum resistance path in the current collector. When the current was collected on the long side (Figure IV.2b), stack resistance was approximately 0.15 mΩ higher than for the current path connected on the short side (Figure IV.2a).

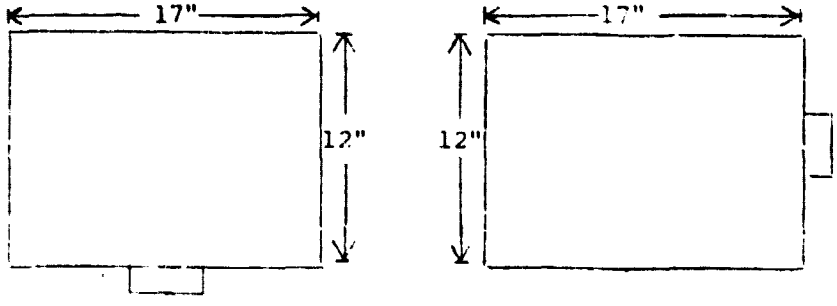

FIGURE IV.2 STACK CURRENT COLLECTING POSITIONS

TABLE IV.1 SUMMARY OF 5 CELL, 1200 CM^2 STACK TESTING

STACK NO.	ASSEMBLY DESCRIPTION	INITIAL AVERAGE PERFORMANCE, volts	OPERATING TIME, hours	REMARKS
407	Rolled electrodes, Kynol matrix	0.59	1243	Required consistent addition of acid. Disassembled.
409	Sheet mold electrodes, Kynol matrix	0.59	56	Crossleaks. Disassembled.
411	Rolled electrodes Kynol matrix	0.56	112	Crossleaks. Disassembled.
412	Sheet mold electrodes, SiC matrix, central current collector	0.62	55	Crossleaks. To be disassembled.

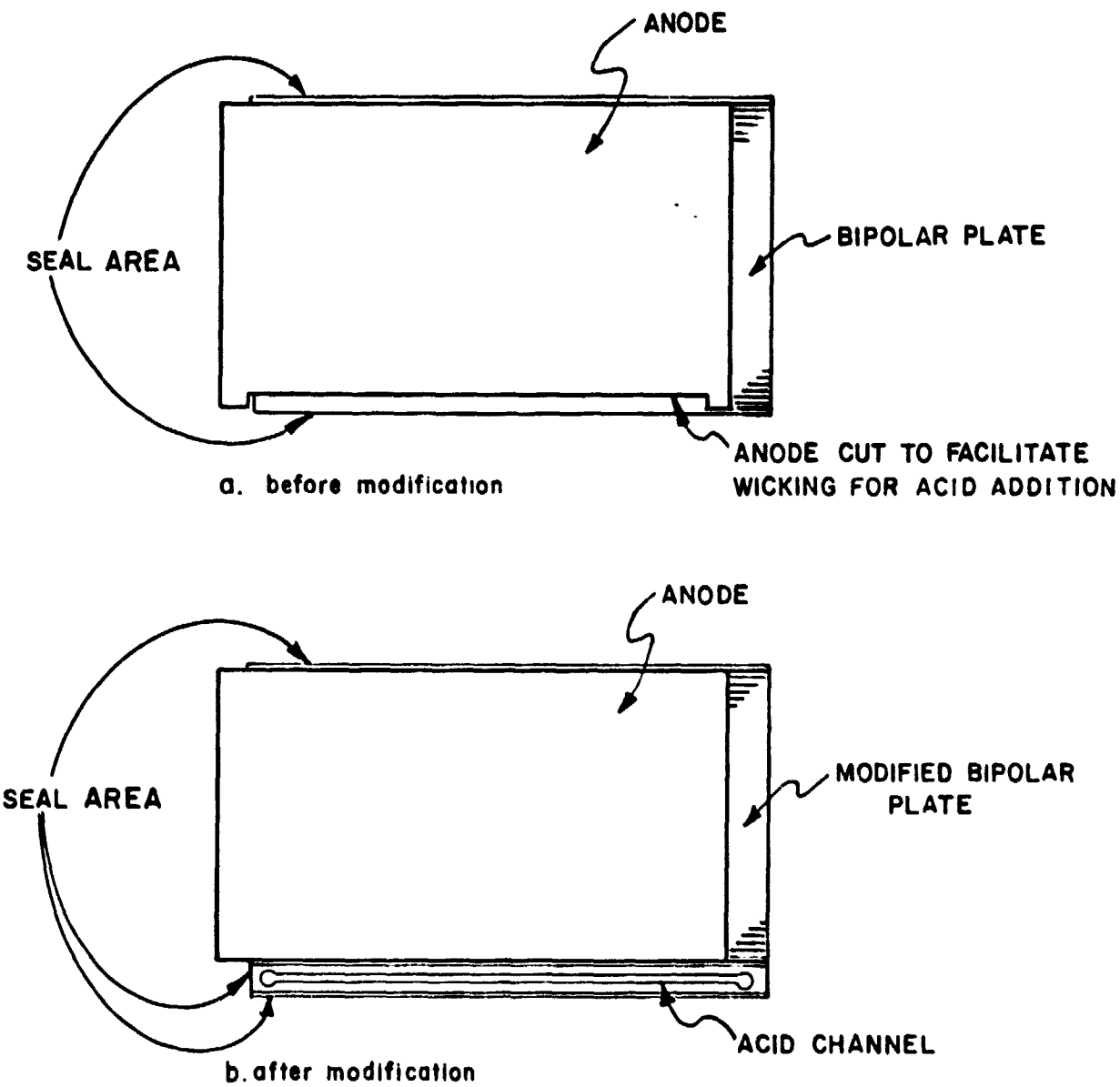

FIGURE IV.1 BIPOLAR PLATE DESIGN MODIFICATION

A theoretical calculation of the resistance for copper at 177°C for these two paths indicates a difference of only 0.16 mΩ between these positions. The voltage drop due to this resistance is 38 mV at 200 mA/cm^2. Similar tab positions on a 350 cm^2 stack indicated a difference of about 0.6 mΩ which corresponds to a 48 mV drop at 200 mA/cm^2. A collector post at the center of the current collector is expected to minimize these losses. The effect of this loss will be smaller as the number of cells in the stack increases. The overall advantages of having a center current collector are described as follows:

- Copper sheet tabs extended to the sides may create gas leaks. The collector post at the center is expected to minimize this problem.
- The center current collector can be made stronger so that it is not susceptible to breakage from wear and tear.
- Less fire hazard can be expected with the center collector than a side collector.

Hence future stacks will incorporate one such current collection design on each side of the stack.

TASK V LONG STACK TESTING

5.1 A 2kW STACK

As reported previously, the first 23-cell stack with DIGAS cooling plates (No. 408) exhibited crossleakage in the cells and a high stack ohmic resistance. Severe electrolyte flooding in air and fuel channels was observed, seemingly caused by crushed carbon backing papers under high compression (~80 psi). Since no improvement in performance was made, the stack was disassembled.

The second 23 cell stack (No. 410) was redesigned with modified compression bars, air ducts and manifolds (as shown in Figure V.1) to improve air flows. The parallel configuration of compression bars used in Stack 408 limited the air manifold depth and also made installation and removal of the manifold cumbersome.

With X-type compression bars (Figure V.1), manifolds can be extended to a greater depth to achieve uniform air distribution. Air ducts were also redesigned to reduce flow resistance. In Stack 408, the exhaust air was turning 90 degrees before exiting and thus exerted a high back pressure. The new design provides an increased air flow rate (up 35%) from 1.34×10^6 to 1.81×10^6 cm^3/min (from 22 to 30 stoich). At the improved air flow, recycling of up to 50% exhaust air could be achieved without a significant performance decrease (previously 10% recycle was the maximum).

In the fuel inlet manifold, a diffuser (Figure V.2) was installed to achieve a uniform fuel distribution, thus allowing high fuel utilization.

To reduce acid squeeze-out from the cells, a startup procedure was followed. Cells wicked at higher temperatures will have highly concentrated acid in the electrodes and matrices. Once the stack is operated at a certain current load, the acid

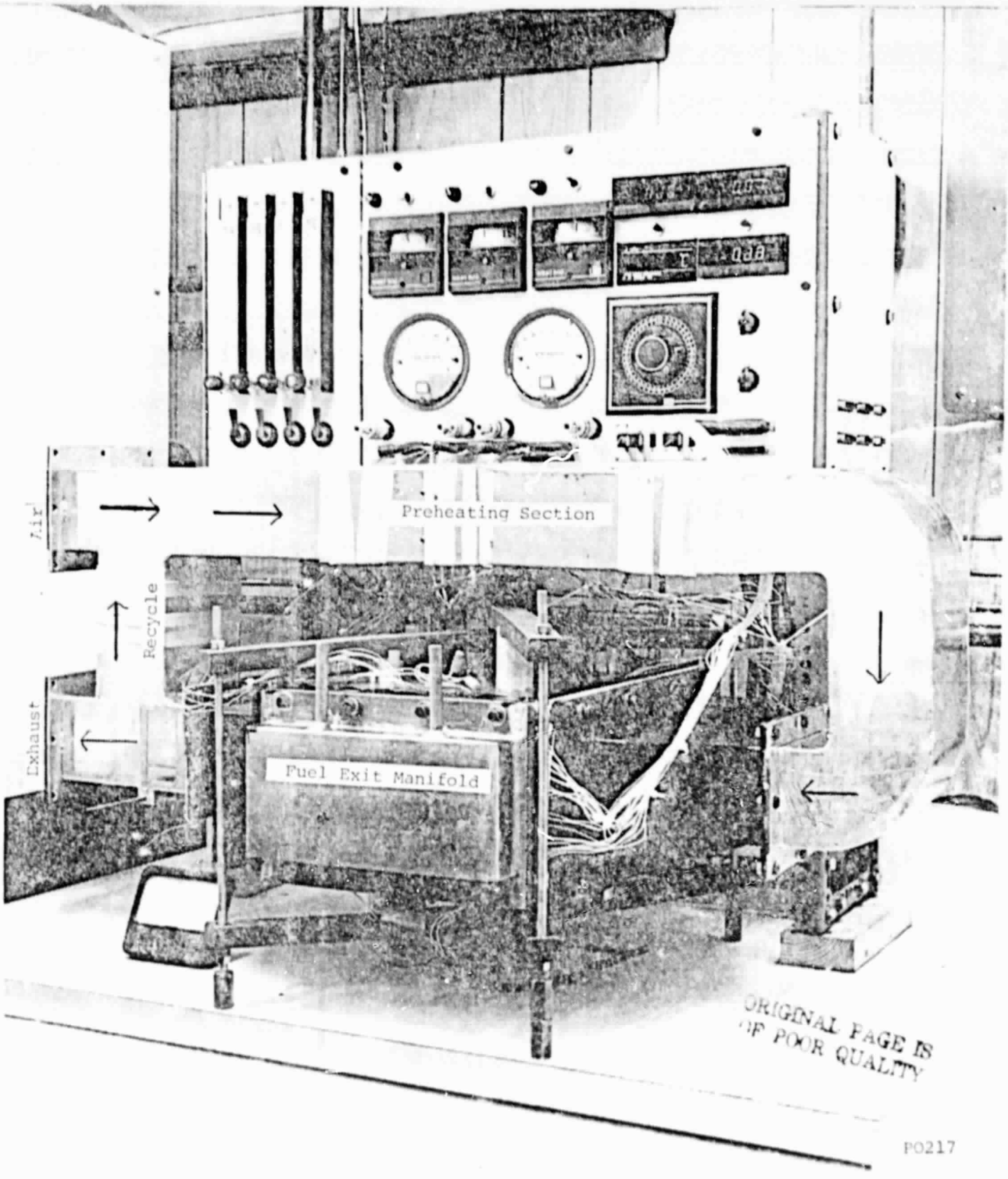

FIGURE V.1 SECOND 2kW STACK ASSEMBLY

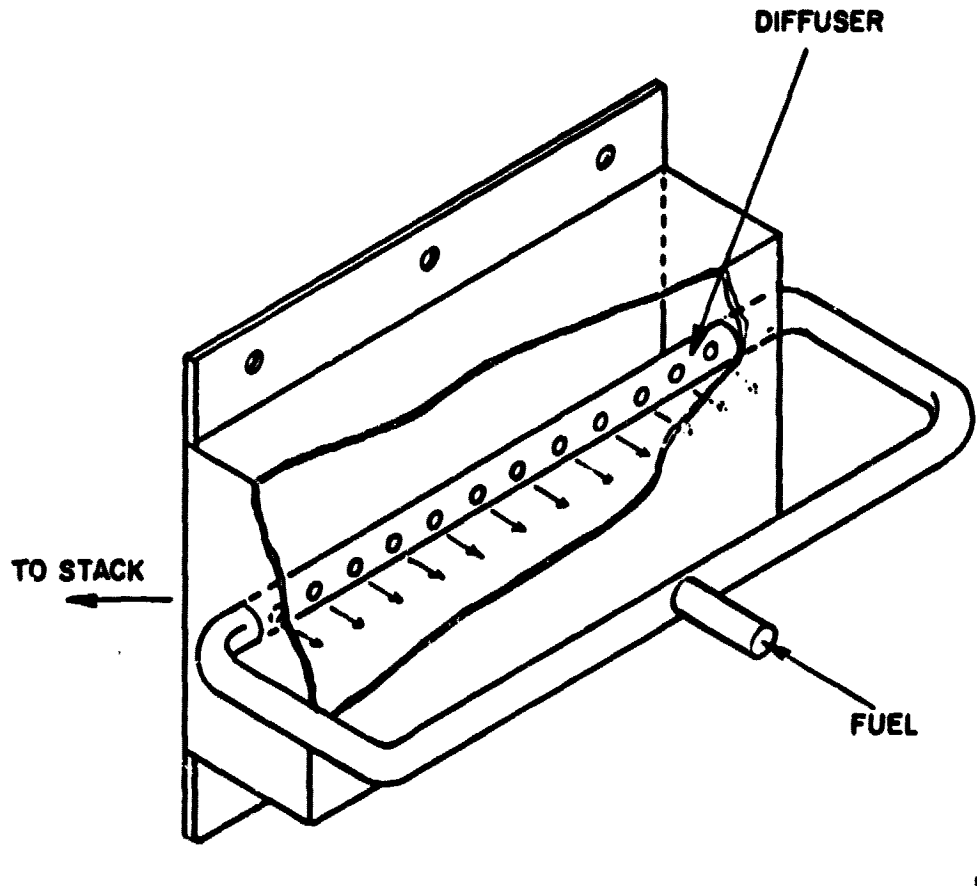

FIGURE V.2 FUEL DIFFUSER IN FUEL MANIFOLD

will be diluted and eventually a considerable amount of acid is squeezed out from the cells. Certainly there will be an optimum wicking temperature under a constant humidity. The work to establish optimal wicking and startup procedures is being pursued*. Roughly estimated parameters have been chosen and applied to the second stack. In the first stack, the wicking temperature was 125°C and the stack was loaded immediately after OCV measurement at that temperature. This resulted in flooding of acid inside the stack (visual observation after taking manifolds apart). For the second stack, the wicking temperature was reduced to 66°C and the stack was loaded (30A) at 150°C. This stack showed no such acid drippage in the manifolds. Figure V.3 shows a plot of acid wicking time vs ohmic resistance for the 2kW stack at 66°C and wicking height as a function of time for an out-of-cell phenolic matrix strip (2.5 x 30.5 cm) at 29°C. For the two cases, the wicking time is almost identical. For the 2kW stack, the total stack resistance was continuously monitored until steady values were obtained after 7 days of wicking. Although the wicking in Stack 410 improved over Stack 408, further wicking studies are needed to ensure uniform wicking.

Table V.1 summarizes ERC testing of the second 23 cell stack. (Refer to the history of stack running in Figure V.4.) As shown, relatively good performance has been achieved: peak performance at 100 mA/cm^2 was 580 mV/cell and slowly decreased as the acid in the matrix and electrodes was depleted. Initial stack ohmic resistance was 12.4 mΩ at 177°C which is lower than the projected values from the 5-cell 1200 cm^2 stack (16 mΩ). Cell running conditions before and after acid depletion are illustrated in Figure V.5. Once the acid is dried up, performance at OCV and at load drops rapidly; after replenishment with acid, the initial performance is regained. During the initial 40 hour endurance test, two acid replenishments were made. The acid loss seems

*ERC 4th Quarterly Progress Report, DEN3-67, September 1979.

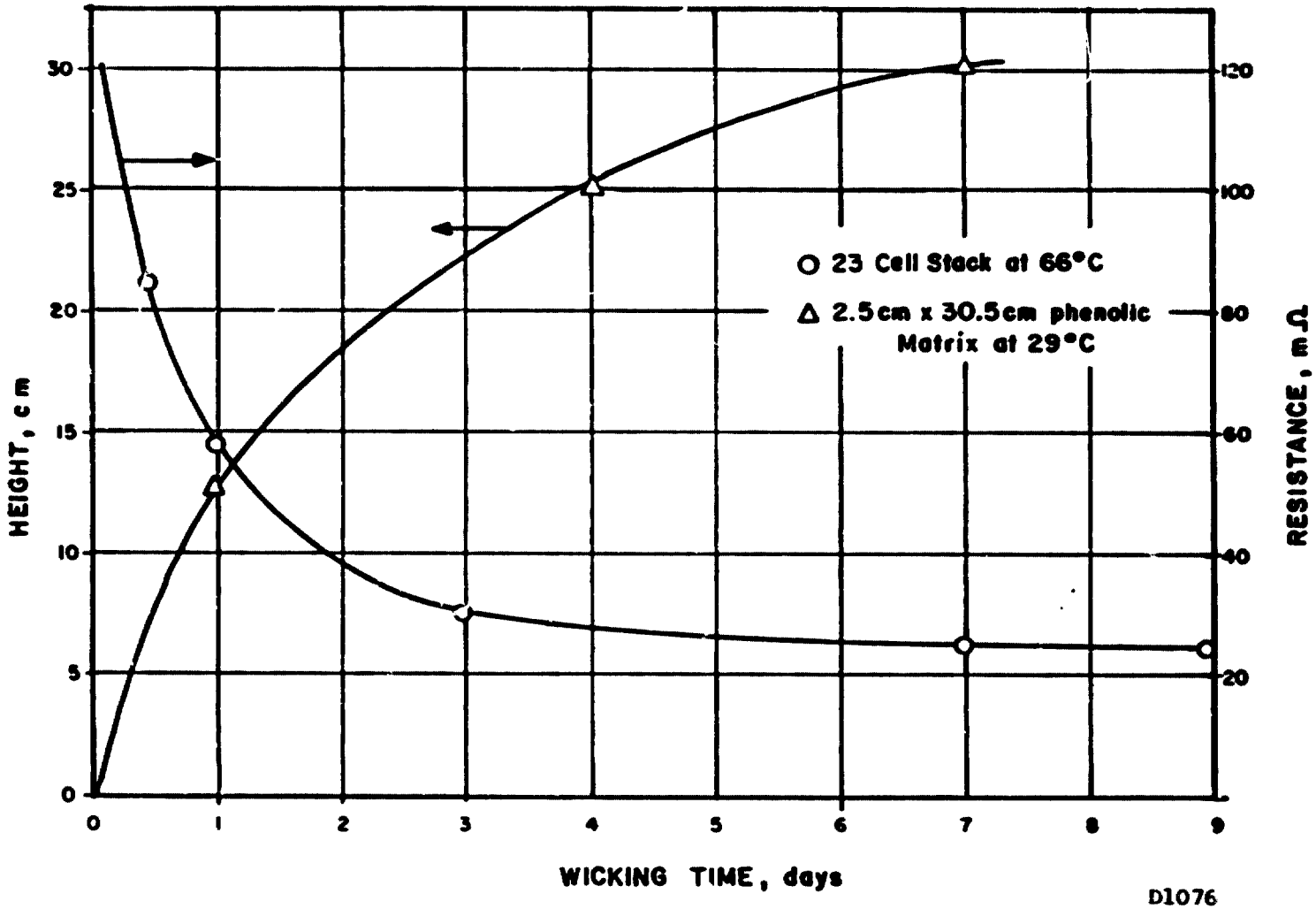

FIGURE V.3 ACID WICKING IN 23-CELL STACK AND A PHENOLIC MATRIX STRIP

TABLE V.1 TEST SUMMARY OF 2KW STACK (No. 410)

RUN NO.	TEST OBJECTIVE	HOURS RUN	BEHAVIOR & PERFORMANCE, volts	CAUSE OF TERMINATION OF RUN	COMMENTS
1	OCV vs wicking	-	Total OCV = 18.67 at 66°C Average Cell OCV = 0.81 Observed crossleak	Insufficient wicking	Wicked for 10 days at 66°C. Stack resistance = 25 mΩ at 66°C.
2	Acid drippage vs starting temperature	2	Started at 149°C. Less acid squeezed out. Total OCV = 20.08 at 177°C Total E = 12.40 at 117A Cell Voltage: Average = 0.54 Lowest = 0.48 Highest = 0.57	Inspection for acid drippage	Rewicked for 3 more days. Current load was slowly increased from 20 to 117A. Observed no crossleak. Stack resistance = 12.4 mΩ at 177°C.
3	Initial endurance	11	Improved performance Total OCV = 17.72 at end of run Total E = 12.94 at 117A. Cell Voltage: Average = 0.56 Lowest = 0.52 Highest = 0.61	Depletion of acid (crossleak & short circuit)	After 11 hours, Cells 1 & 2 showed negative voltage. Stack resistance = 18 mΩ. Hottest spot = 180°C.
4	OCV & performance vs rewicking and acid drippage vs wicking temp.	1	No crossleak Total OCV = 19.30 at 149°C. Total E = 12.94 at 117A. Cell Voltage: Average = 0.56 Lowest = 0.40 Highest = 0.61	Inspection for acid drippage	Rewicked for 4 days at 82°C. Stack resistance = 13 mΩ at 177°C. Hottest spot = 184°C. More acid wetting around manifolds than 66°C wicking

TABLE V.1 TEST SUMMARY OF 2kW STACK (No. 410)

RUN NO.	TEST OBJECTIVE	HOURS RUN	BEHAVIOR & PERFORMANCE, volts	CAUSE OF TERMINATION OF RUN	COMMENTS
5	Performance vs recycling of exhaust air	1	Total E = 13.09 at 115A at 50% recycle Total E = 13.17 at zero recycle Cell Voltage: Lowest = 0.46 Highest = 0.62	Continue for endurance test	ΔP = 3.05 cm H_2O on air side ΔP = 0.2 cm H_2O on H_2 side Stack resistance = 12 mΩ Hottest spot = 186°C
6	Endurance	13	Initial E = 13.09 Final E = 12.90 at 113A Cell Voltage: Lowest changed from 0.46 to 0.39 Highest changed from 0.62 to 0.61	Lowered performance at Cell 1	Best voltage at Cell 21. Hottest spot = 182°C.
7	Endurance	12	Initial OCV = 18.63 at 177°C Initial E = 12.92 at 113A Final OCV = 17.21 Final E = 12.70 at 113A Cell Voltage: Lowest changed from 0.49 to 0.64 Highest remained at 0.61	Depletion of acid (crossleak). Overheating	Best voltage at Cell 22. Hottest spot 197°C. Worst crossleak.

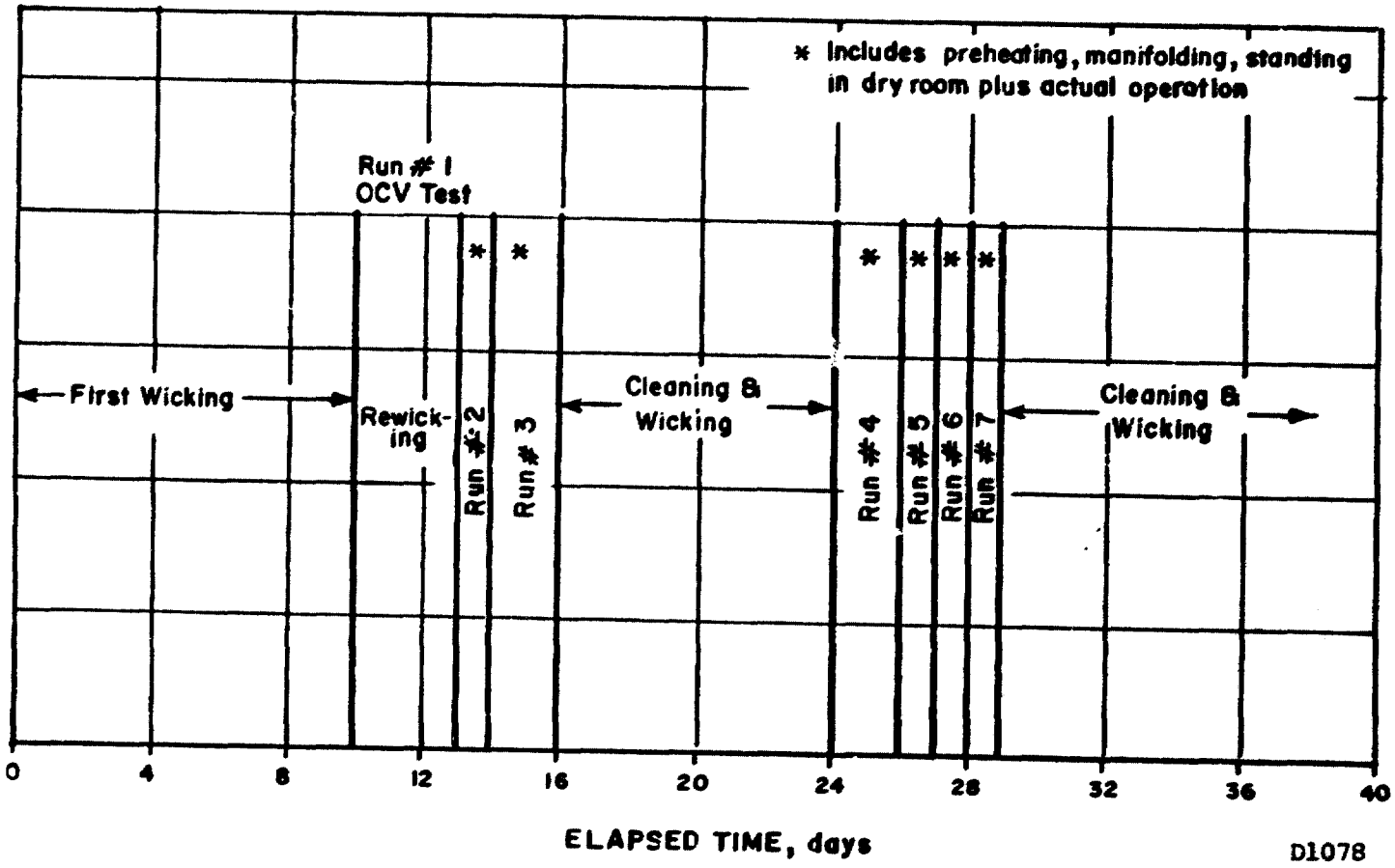

FIGURE V.4 HISTORY OF STACK 410 OPERATION

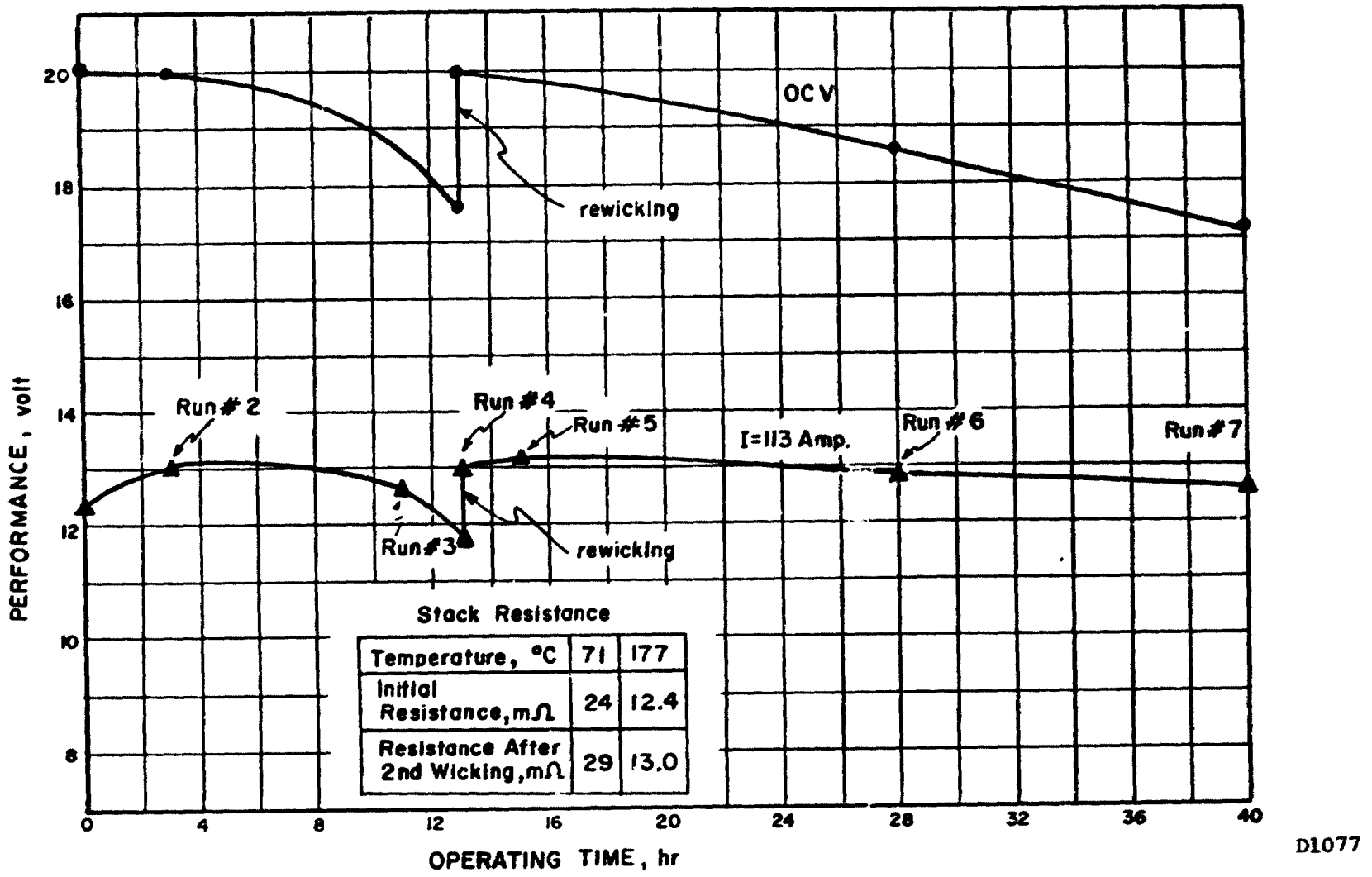

FIGURE V.5 PERFORMANCE CHARACTERISTICS WITH RUNNING TIME FOR 2nd 2kw STACK

very high, probably due to the high air flow rate, necessitating the inclusion of a built-in reservoir to maintain the acid level. For the next stack, acid wicking channels will be built into the bipolar plates to replenish acid while the stack is running.

For temperature profiles in the stack, refer to Figure V.6. The fuel side shows a very uniform temperature distribution. The small temperature gradients on the air side compared to the previous stack (No. 408) are attributed to improved stack manifolding. For the next stack, the acid reservoir and sealing problems will be addressed.

5.2 THERMAL STACK EXPANSION/CONTRACTION

Thermal stack expansion (in the range of stack operating temperatures) was measured at four corners of the stack. Table V.2 summarizes the averaged stack expansions for four different stack temperatures. From 100 to 174°C, a total stack expansion of 0.036 cm was observed, half of which comes from the active cell height as shown in the table. To maintain a constant compression on the stack (50 psi), the stack should therefore be adjusted by 0.036 cm at 174°C. This type of information will be used for keeping the cell components in good contact during temperature variations.

TABLE V.2 THERMAL EXPANSION FOR A 23-CELL STACK

TEMPERATURE, °C	DIMENSION A, cm (active cell ht)	DIMENSION B, cm (total stack height including end plates)
100	13.790	21.224
125	13.792	21.237
140	13.795	21.247
174	13.807	21.260

Stack Compression = 50 psi at 100°C

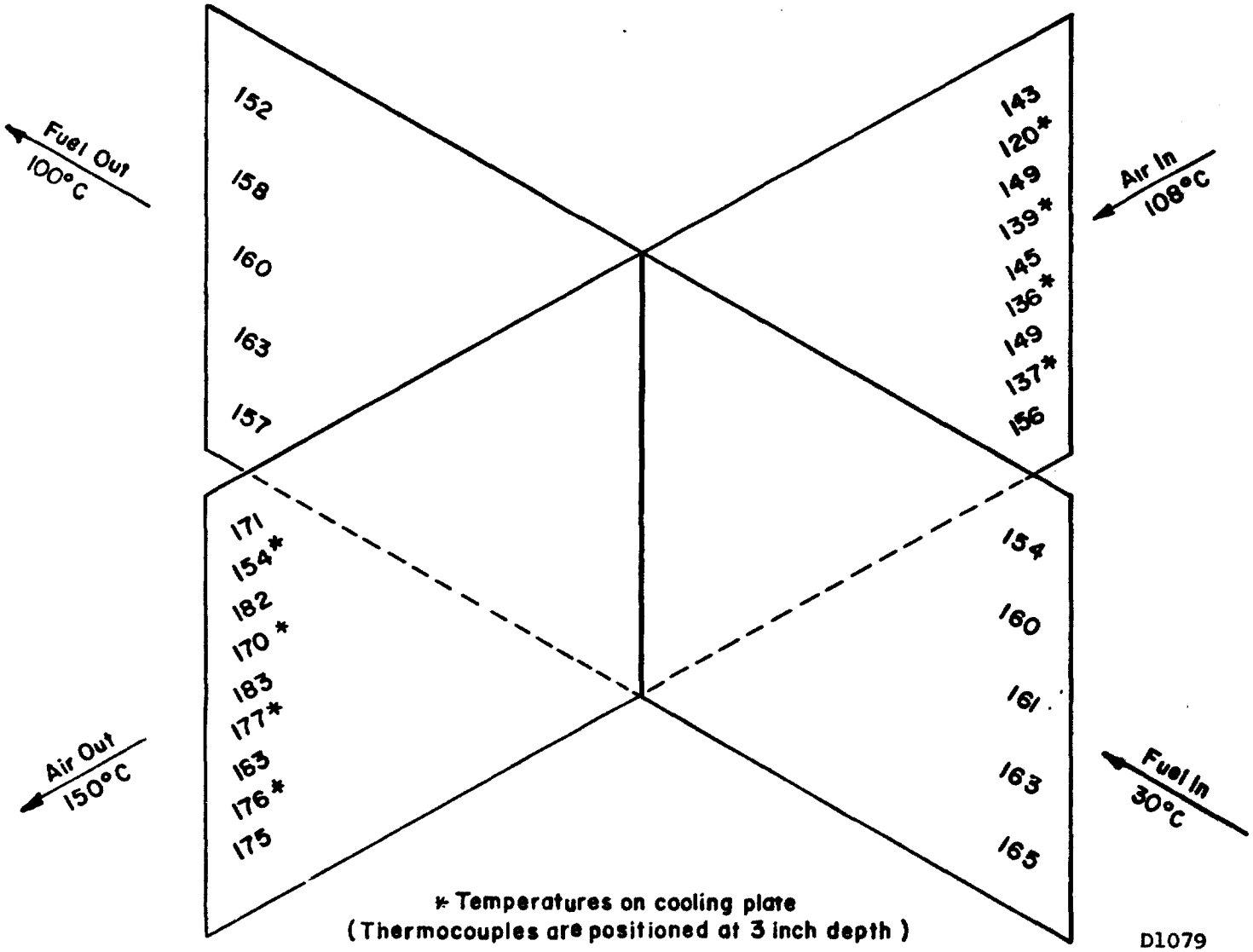

FIGURE V.6 TEMPERATURE PROFILES ON CENTER PLANES OF 2kW STACK
(measured at E = 12.90 V and I = 112 A)

5.3 REFORMER TESTING

The steam reformer was tested for performance with propane and methane fuel at various space velocities. For propane fuel, a space velocity of 355 hr^{-1} showed a trace of unconverted propane in the reformed product at 516°C. Figures V.7 and V.8 show temperature profiles along the reformer tube for the given space velocities. The asymptotic behavior of the temperature in the catalyst bed suggests the establishment of equilibrium. Table V.3 compares the experimental product compositions with equilibrium calculations at the reformer exit temperatures. As shown, the reformer is close to equilibrium operation. To produce the hydrogen required for a 2kW stack, the propane space velocity in the present reactor is 455 hr^{-1}. At this space velocity, a reforming temperature of 649°C is expected for 100% fuel conversion. Table V.4 compares reformed gas compositions between experimental and equilibrium calculations for pure methane fuel. As shown in the table, space velocities up to 705 hr^{-1} lead to equilibrium condition at a reforming temperature of 593°C according to equilibrium calculations. As the space velocity goes above 705 hr^{-1}, the reforming reactions seem to fall behind equilibrium. To achieve a 2kW hydrogen supply, an approximate methane space velocity of 1100 hr^{-1} is required (based on 100% conversion). In the present test, 76% fuel conversion was achieved for a space velocity of 1135 hr^{-1} at an exit gas temperature of 615°C. For 100% conversion, a reforming temperature of 700°C is required (from equilibrium analysis). While constructing a contaminant guard bed and shift converter, optimal operating parameters will be determined to meet the 2kW stack fuel supply rerquirements, based on theoretical analysis.

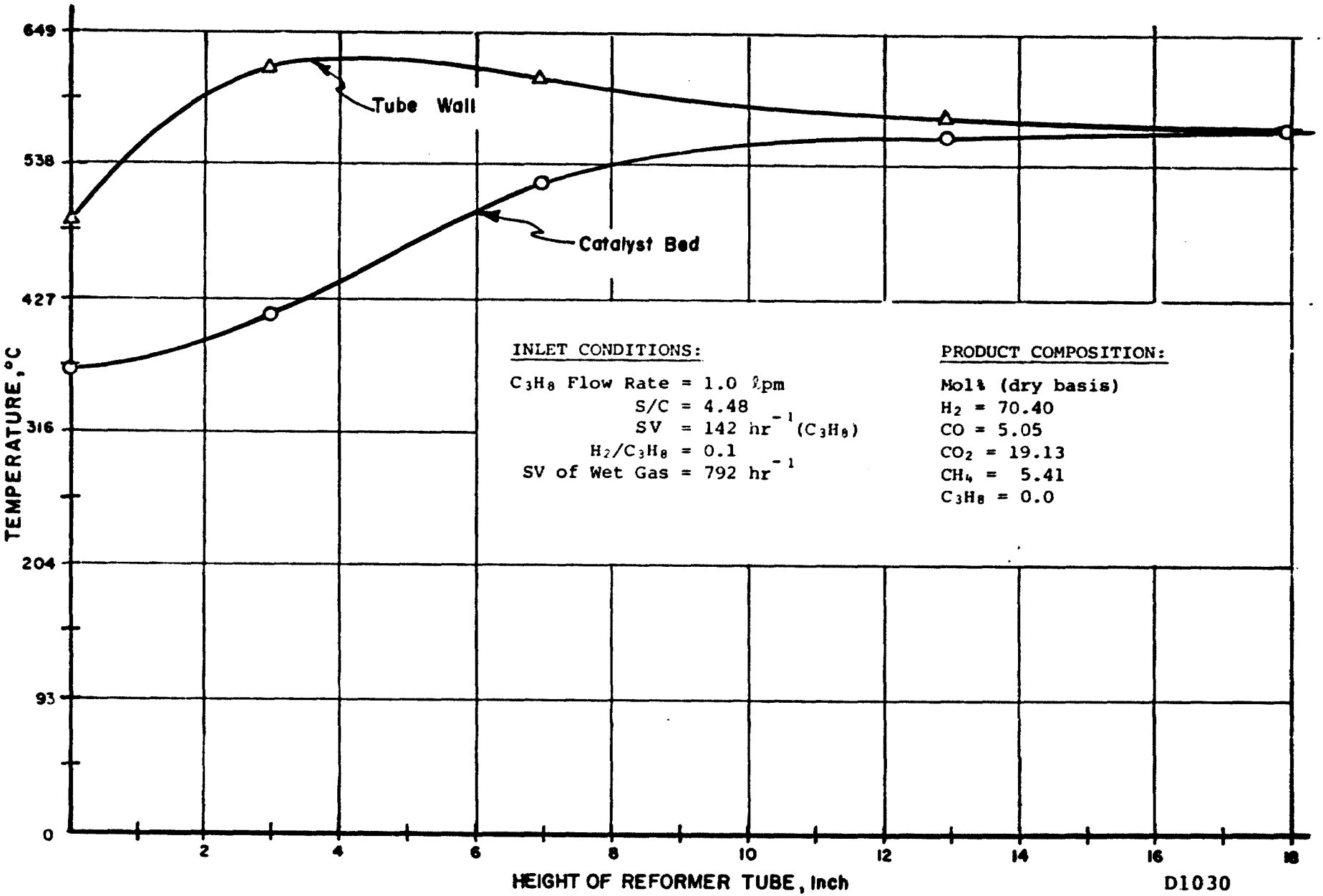

FIGURE V.7 THERMAL CHARACTERISTICS IN PROPANE REFORMING AT A FLOW RATE OF 1.0 LPM

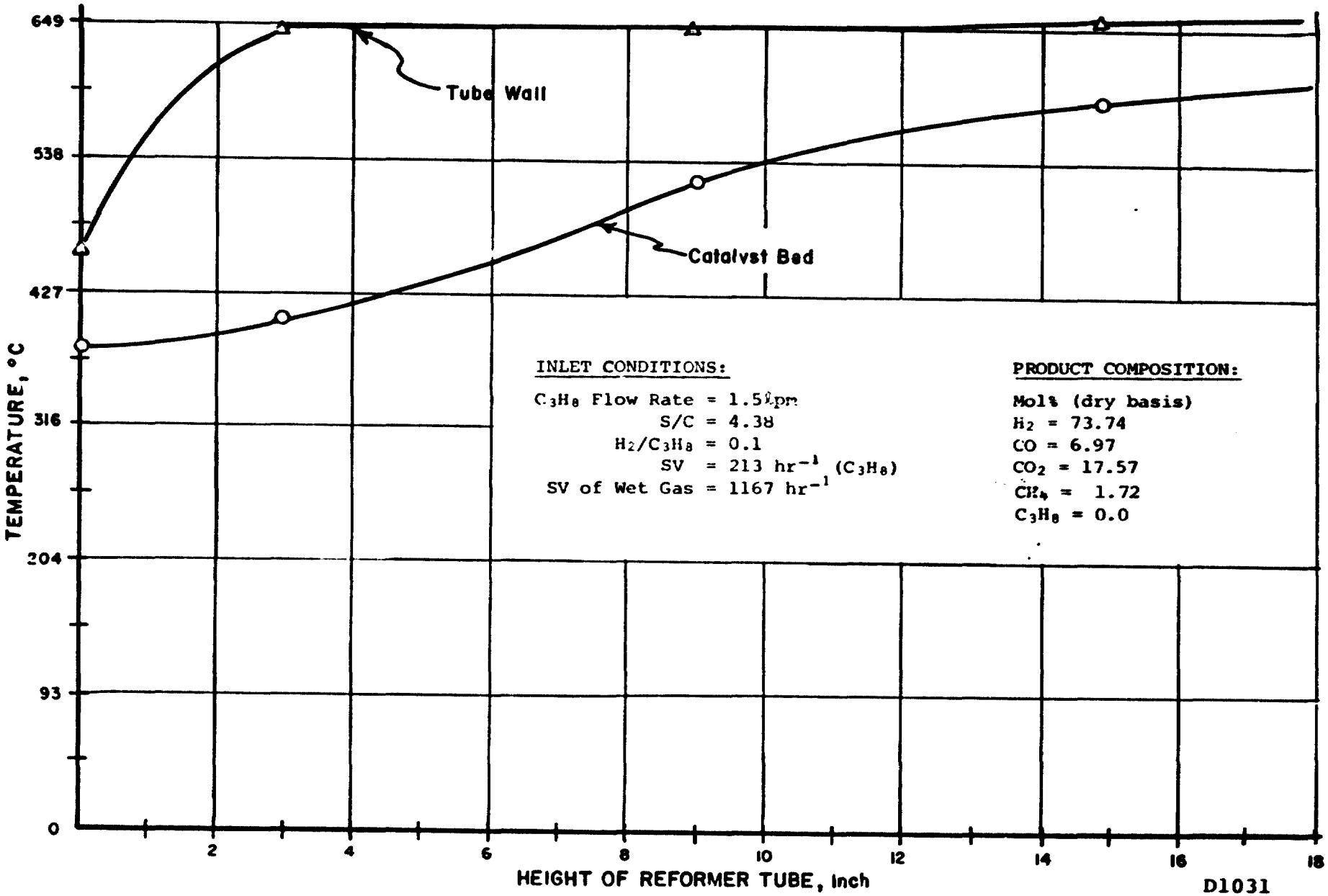

FIGURE V.8 THERMAL CHARACTERISTICS IN PROPANE REFORMING AT A FLOW RATE OF 1.5 LPM

TABLE V.3 COMPARISON OF EXPERIMENTAL COMPOSITIONS WITH EQUILIBRIUM CALCULATION FOR PROPANE PERFORMING

Reformer Conditions	Component	Exit Composition, Mol fr. (Dry Basis)	
		Experimental	Calculated*
T_{in} = 371°C	H_2	0.70	0.72
T_{out} = 566°C	CO	0.05	0.05
S/C = 4.48	CO_2	0.19	0.18
$(H_2)_o$ = 0.1	CH_4	0.05	0.05
SV† = 142 hr^{-1}	C_3H_8	0	0
T_{in} = 238°C	H_2	0.65	0.66
T_{out} = 516°C	CO	0.02	0.03
S/C = 4.35	CO_2	0.21	0.20
$(H_2)_o$ = 0.1	CH_4	0.11	0.11
SV† = 355 hr^{-1}	C_3H_8	0.01	0
T_{in} = 382°C	H_2	0.74	0.73
T_{out} = 604°C	CO	0.07	0.07
S/C = 4.38	CO_2	0.18	0.17
$(H_2)_o$ = 0.1	CH_4	0.02	0.02
SV† = 213 hr^{-1}	C_3H_8	0	0
T_{in} = 357°C	H_2	0.73	0.74
T_{out} = 604°C	CO	0.06	0.07
S/C = 4.41	CO_2	0.18	0.17
$(H_2)_o$ = 0.1	CH_4	0.03	0.02
SV† = 284 hr^{-1}	C_3H_8	0	0

* Based on reformer exit temperature

† Space velocities are for propane at NTP

TABLE V.4 COMPARISON OF REFORMED PRODUCT COMPOSITIONS OBTAINED BY EXPERIMENT AND BY EQUILIBRIUM CALCULATION FOR METHANE REFORMING

INLET GAS	EXIT TEMP °C	EXIT GAS COMPOSITION, Mol fr. (Day Basis)		EQUILIBRIUM CONSTANT			
				REFORMING		SHIFT	
		Exptl.	Eqm. Calc.	Exptl.	Thermo-dyn.	Exptl.	Thermo-dyn.
H_2O/C = 4.42 H_2/C = 0.1 SV = 565 hr^{-1} (CH_4) at NTP	593	CH_4 = 0.03 CO = 0.06 CO_2 = 0.14 H_2 = 0.77 X* = 87.56%	0.04 0.06 0.14 0.77 85.06%	0.49	0.37	2.84	2.59
H_2O/C = 4.35 H_2/C = 0.1 SV = 705 hr^{-1}	601	CH_4 = 0.03 CO = 0.06 CO_2 = 0.14 H_2 = 0.77 X* = 88.27%	0.03 0.06 0.14 0.77 86.9%	0.57	0.51	2.92	2.46
H_2O/C = 4.42 H_2/C = 0.1 SV = 848 hr^{-1}	593	CH_4 = 0.04 CO = 0.05 CO_2 = 0.14 H_2 = 0.76 X* = 82.11%	0.04 0.06 0.14 0.77 85.06%	0.26	0.37	2.79	2.59
H_2O/C = 4.37 H_2/C = 0.1 SV = 990 hr^{-1}	610	CH_4 = 0.04 CO = 0.07 CO_2 = 0.13 H_2 = 0.76 X* = 82.18%	0.03 0.07 0.14 0.77 89.08%	0.30	0.68	2.10	2.36
H_2O/C = 3.31 H_2/C = 0.1 SV = 1135 hr^{-1}	615	CH_4 = 0.06 CO = 0.08 CO_2 = 0.12 H_2 = 0.74 X* = 75.9%	0.04 0.08 0.12 0.76 83.39%	0.39	0.83	2.01	2.29

*CH_4 conversion